Monthly Notices
of the
ROYAL ASTRONOMICAL SOCIETY

MNRAS **446,** 4078–4087 (2015) doi:10.1093/mnras/stu2388

New white dwarf stars in the Sloan Digital Sky Survey Data Release 10

S. O. Kepler,[1]★ I. Pelisoli,[1] D. Koester,[2] G. Ourique,[1] S. J. Kleinman,[3] A. D. Romero,[1] A. Nitta,[3] D. J. Eisenstein,[4] J. E. S. Costa,[1] B. Külebi,[5,6] S. Jordan,[7] P. Dufour,[8] Paolo Giommi[9] and Alberto Rebassa-Mansergas[10]

[1]*Instituto de Física, Universidade Federal do Rio Grande do Sul, 91501-900 Porto-Alegre, RS, Brazil*
[2]*Institut für Theoretische Physik und Astrophysik, Universität Kiel, D-24098 Kiel, Germany*
[3]*Gemini Observatory, Hilo, HI 96720, USA*
[4]*Harvard–Smithsonian Center for Astrophysics, 60 Garden St, MS #20, Cambridge, MA 02138, USA*
[5]*Institut de Ciències de L'Espai, Universitat Autònoma de Barcelona, E-08193 Bellaterra, Spain*
[6]*Institute for Space Studies of Catalonia, c/Gran Capità 2-4, Edif. Nexus 104, E-08034 Barcelona, Spain*
[7]*Astronomisches Rechen-Institut, Zentrum für Astronomie der Universität Heidelberg, Mönchhofstr. 12-14, D-69120 Heidelberg, Germany*
[8]*Département de Physique, Université de Montréal, C. P. 6128, Succ. Centre-Ville, Montréal, QC H3C 3J7, Canada*
[9]*ASDC Agenzia Spaziale Italiana, Via del Politecnico snc, I-00133 Rome, Italy*
[10]*Kavli Institute for Astronomy and Astrophysics, Peking University, Beijing 100871, People's Republic of China*

Accepted 2014 November 8. Received 2014 November 8; in original form 2014 July 28

ABSTRACT

We report the discovery of 9088 new spectroscopically confirmed white dwarfs and subdwarfs in the Sloan Digital Sky Survey Data Release 10. We obtain $T_{\rm eff}$, log g and mass for hydrogen atmosphere white dwarf stars (DAs) and helium atmosphere white dwarf stars (DBs), and estimate the calcium/helium abundances for the white dwarf stars with metallic lines (DZs) and carbon/helium for carbon-dominated spectra DQs. We found 1 central star of a planetary nebula, 2 new oxygen spectra on helium atmosphere white dwarfs, 71 DQs, 42 hot DO/PG1159s, 171 white dwarf+main-sequence star binaries, 206 magnetic DAHs, 327 continuum-dominated DCs, 397 metal-polluted white dwarfs, 450 helium-dominated white dwarfs, 647 subdwarfs and 6887 new hydrogen-dominated white dwarf stars.

Key words: catalogues – stars: magnetic field – subdwarfs – white dwarfs.

1 INTRODUCTION

White dwarf stars are the end product of evolution of all stars with progenitor masses below 8–10.5 $M_{\odot}$, depending on metallicity (Doherty et al. 2014). The first full white dwarf catalogue from Sloan Digital Sky Survey (SDSS) data (Kleinman et al. 2004) was based on SDSS Data Release 1 (DR1; Abazajian et al. 2003). Using data from the SDSS Data Release 4 (DR4; Adelman-McCarthy et al. 2006), Eisenstein et al. (2006) reported over 9000 spectroscopically confirmed white dwarfs stars. In the latest white dwarf catalogue based on the SDSS Data Release 7 (DR7), Kleinman et al. (2013) classified the spectra of 19 713 white dwarf stars, of which 12 831 were hydrogen atmosphere white dwarf stars (DAs) and 922 helium atmosphere white dwarf stars (DBs), including the (re)analysis of stars from previous releases.

The SDSS data massively increased the number of known white dwarfs, which had an enormous impact on the knowledge of these stars. However, target selection considerations of the original SDSS implied that white dwarf selection for spectroscopy was incomplete. White dwarf stars were targeted in SDSS-III's (Eisenstein et al. 2011) Baryon Oscillation Spectroscopic Survey (BOSS) by the ancillary project White Dwarf and Hot Subdwarfs (Dawson et al. 2013). By Data Release 10 (DR10), the ancillary target programme obtained the spectra of 3104 colour-selected white dwarf candidates that were missed by prior SDSS spectroscopic surveys. Here, we report on our full search for new white dwarfs from the SDSS DR10 (Ahn et al. 2014). Our catalogue does not include stars from the earlier catalogues.

2 TARGET SELECTION

SDSS multicolour imaging separates hot white dwarf and subdwarf stars from the bulk of the stellar and quasar loci in colour–colour space (Harris et al. 2003). Special target classes in SDSS produced the world's largest spectroscopic samples of white dwarfs. However, much of SDSS white dwarf targeting required that the objects be unblended, which caused many brighter white dwarfs to be skipped (for a detailed discussion, see section 5.6 of Eisenstein et al. 2006). The BOSS ancillary targeting programme (Dawson et al. 2013) relaxed this requirement and imposed colour cuts to focus on warm

★ E-mail: kepler@if.ufrgs.br

and hot white dwarfs. Importantly, the BOSS spectral range extends further into the UV, allowing full coverage of the Balmer lines.

The targeted white dwarfs were required to be point sources with clean photometry, and to have USNO-B Catalog counterparts (Monet et al. 2003). They were also restricted to regions inside the DR7 imaging footprint and required to have colours within the ranges $g < 19.2$, $(u - r) < 0.4$, $-1 < (u - g) < 0.3$, $-1 < (g - r) < 0.5$ and to have low Galactic extinction $A_r < 0.5$ mag. Additionally, targets that did not have $(u - r) < -0.1$ and $(g - r) < -0.1$ were required to have USNO proper motions larger than 2 arcsec per century. Objects satisfying the selection criteria that had not been observed previously by the SDSS were denoted by the WHITEDWARF_NEW target flag, while those with prior SDSS spectra are assigned the WHITEDWARF_SDSS flag. Some of the latter were re-observed with BOSS in order to obtain the extended wavelength coverage that the BOSS spectrograph offers.

The colour selection used includes DA stars with temperatures above ∼14 000 K, helium atmosphere white dwarfs above ∼8000 K, as well as many rarer classes of white dwarfs. Hot subdwarfs (sdB and sdO) were targeted as well.

SDSS-III BOSS (Dawson et al. 2013) optical spectra extends from 3610 to 10 140 Å, with spectral resolution 1560–2270 in the blue channel, and 1850–2650 in the red channel (Smee et al. 2013). The data were reduced by the spectroscopic reduction pipeline of Bolton et al. (2012).

In addition to the 3104 targeted new white dwarf candidates, we selected the spectra of any object classified by the ELODIE pipeline (Bolton et al. 2012) as a white dwarf, which returned 27 372 spectra. Our general colour selection from Kleinman et al. (2013) returned 265 633 spectra of which 42 154 had already been examined in Kleinman et al. (2013). From these, we examined the spectra of additional 12 340 with $g \leq 20$ and no Quasi Stellar Object (QSO) flag. On top of those, we analysed another 35 000 spectra selected on the SDSS 3358 200 optical spectra reported by DR10 with an automated search algorithm loosely based on Si et al. (2014), estimating local averages at 75 pre-selected wavelengths sampling white dwarf strong lines, and found another 1010 stars. Of the 3104 objects targeted specifically as new white dwarf spectra by BOSS as an ancillary programme, 574 were not identified as white dwarfs or subdwarfs by us. From the total inspected by eye, around 37 per cent of the selected spectra are in fact confirmed white dwarfs, of which 20 per cent were already known. Kleinman et al. (2013) reported that 47 per cent of their colour-selected sample are white dwarf stars. Of the Ancillary Program 43 of WHITEDWARF_SDSS already observed, 157 in 2432 colour-selected stars are in fact quasars. These fractions must be considered when using samples of photometrically selected white dwarfs, for example, to calculate luminosity functions.

We applied automated selection techniques supplemented by complete, consistent human identifications of each candidate white dwarf spectrum.

3 DATA ANALYSIS

After visual identification of the spectra as a probable white dwarf, we first fitted the optical spectra to DA and DB local thermodynamic equilibrium (LTE) grids of synthetic non-magnetic spectra derived from model atmospheres (Koester 2010). The DA model grid uses the ML2/$\alpha = 0.6$ approximation, and for the DBs, we use the ML2/$\alpha = 1.25$ approximation, to be consistent with Kleinman et al. (2013). Our DA grid extends up to $T_{\rm eff} = 100\,000$ K, considering Napiwotzki (1997) concluded pure hydrogen atmospheres of DA white dwarfs are well represented by LTE calculations for effective temperatures up to 80 000 K. Only when traces of helium are present, non-local thermodynamic equilibrium (NLTE) effects on the Balmer lines occur, down to effective temperatures of 40 000 K, recommending the neglect of traces of helium in the LTE models for the analysis of DA white dwarfs. We fitted all candidate white dwarf spectra and colours with the AUTOFIT code described in Kleinman et al. (2004), Eisenstein et al. (2006) and Kleinman et al. (2013). AUTOFIT fits only clean DA and DB models, so it does not recognize other types of white dwarf stars. In addition to the best-fitting model parameters, it also outputs a goodness-of-fit estimate and several quality control checks and flags for other features noted in the spectrum or fit. The automatic fits include SDSS imaging photometry and allow for refluxing of the models by a low-order polynomial to incorporate effects of unknown reddening and spectrophotometric flux calibration errors. In addition, we have also fitted the spectral lines and photometry separately (Koester 2010), selecting between the hot and cool solutions using photometry as an indicator. We make use of the latest SDSS reductions for photometry and spectroscopy. The white dwarf model atmospheres in our AUTOFIT spectral fits, providing reliable $\log g$ and $T_{\rm eff}$ determinations for each identified clean DA and DB are the same used in Kleinman et al. (2013). We use the word *clean* to identify spectra that show only features of non-magnetic, non-mixed, DA or DB (and DBA) stars.

We did not further restrict our sample by magnitude. The SDSS spectra we classified as white dwarfs or subdwarfs have a g-band signal-to-noise ratio $91 \geq {\rm S/N}(g) \geq 1$, with an average of 15. The lowest S/N in the g band occurs for stars cooler than 7000 K, but they have significant S/N in the red part of the spectrum.

3.1 Spectral classification

Because we are interested in obtaining accurate mass distributions for our DA and DB stars, we were conservative in labelling a spectrum as a clean DA or DB, adding additional subtypes and uncertainty notations if we saw signs of other elements, companions or magnetic fields in the spectra. While some of our mixed white dwarf subtypes would probably be identified as clean DAs or DBs with better signal-to-noise spectra, few of our identified clean DAs or DBs would likely be found to have additional spectral features within our detection limit.

We looked for the following features to aid in the classification for each specified white dwarf subtype.

(i) Balmer lines – normally broad and with a Balmer decrement [DA but also DAB, DBA, DZA and subdwarfs]
(ii) He I 4471 Å [DB, subdwarfs]
(iii) He II 4686 Å [DO, PG1159, subdwarfs]
(iv) C2 Swan band or atomic C I lines [DQ]
(v) Ca II H & K [DZ, DAZ]
(vi) C II 4367 Å [HotDQ]
(vii) Zeeman splitting [magnetic white dwarfs]
(viii) featureless spectrum with significant proper motion [DC]
(ix) flux increasing in the red [binary, most probably M companion]
(x) O I 6158 Å [Dox].

We also found a group of stars to have a very steep Balmer decrement (i.e. only a broad Hα and sometimes Hβ is observed while the other lines are absent) that could not be fit with a pure hydrogen grid, or indicated extremely high gravities. We find that

Table 1. Numbers of newly identified white dwarf by type.

No. of stars	Type
6243	DAs[a]
450	DBs[b]
397	DZ
327	DC
234	DAB
206	DAH
247	DAZ
171	WD+MS[c]
71	DQ
62	DAO
42	DO/PG 1159
9	DA-He
2	Dox
1	CSPN
636	sd[d]

[a]Pure DAs. [b]Include DBAs. [c]These spectra show both a white dwarf star and a companion, non-white dwarf spectrum, usually a main-sequence M star. [d]These are sdBs and sdOs subdwarf star spectra.

these objects are best explained as helium-rich DAs, and denote them DA-He.

We finally note that the white dwarf colour space also contains many hot subdwarfs. It is difficult, just by looking at a spectrum, to tell a low-mass white dwarf from a subdwarf, as they are both dominated by hydrogen lines and the small differences in surface gravity cannot be spotted by visual inspection alone. We therefore extended the model grid to $\log g = 4.5$ to separate white dwarfs, hot subdwarfs and main-sequence stars (see Sections 4.3 and 4.7), but the differences in the line widths for DAs cooler than $\simeq$ 8000 K and hotter than $\simeq$ 30 000 K are minor with changing gravity.

3.2 Classification results

Table 1 lists the number of each type of white dwarf star we identified.

The hot helium-dominated spectra of PG 1159 and DO stars with S/N≥10 included in our Table 6 were fitted with NLTE models and reported by Werner, Rauch & Kepler (2014) and Reindl et al. (2014).

4 RESULTS

4.1 Oxygen spectra

Fig. 1 shows the spectra of SDSS J123807.42+374322.4, with 222 ± 5 mas yr^{-1} proper motion, $g = 18.94 \pm 0.01$, and SDSS J152309.05+015138.3, with 167 ± 14 mas yr^{-1} proper motion, $g = 19.37 \pm 0.01$, have spectra dominated by O I lines, that appear much stronger than the C I lines, which can only be explained as being almost naked O–Ne cores, like SDSS J110239.69+205439.38, discovered by Gänsicke et al. (2010).

Theoretically, stars with initial masses $7\,M_\odot \leq M \leq 10\,M_\odot$ will reach sufficiently high core temperatures to proceed to carbon burning, and produce either oxygen–neon (O–Ne) core white dwarfs, or undergo a core-collapse supernova (SNII) via electron capture on

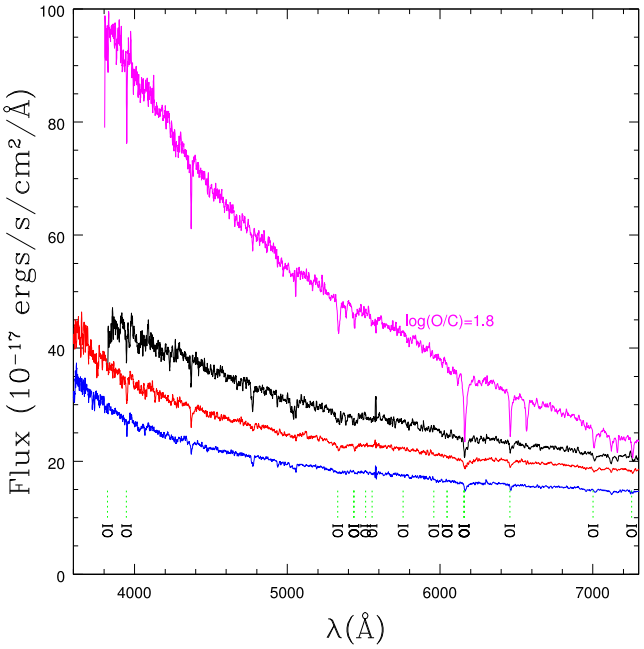

Figure 1. Spectra of the prototype oxygen-dominated atmosphere white dwarf SDSS J110239.69+205439.38=2488−54149−0167 at the top, SDSS J142342.64+572949.3=2547−53917−0283, and the two new SDSS J123807.42+374322.4=3969−55307−0772 and SDSS J152309.05+015138.3=4011−55635−0072.

the products of carbon burning (Nomoto 1984; Doherty et al. 2014). The exact outcome of stellar evolution in this mass range depends critically on the detailed understanding of the nuclear reaction rates involved, mass-loss and on the efficiency of convective mixing in the stellar cores (e.g. Straniero et al. 2003). Observational constraints on stellar models come from analysis of SNII progenitors (Smartt 2009; Smartt et al. 2009; Valenti et al. 2009), suggest a lower limit on the progenitor masses of $8 \pm 1 M_\odot$, but depends on progenitor metallicity.

Denissenkov et al. (2013, 2014) propose the existence of hybrid C/O core white dwarfs with O–Ne envelopes by stars where carbon is ignited off-centre but convective mixing prevents the carbon burning to reach the centre.

4.2 Magnetic fields and Zeeman splittings

Similar to those reported for DR7 in Kleinman et al. (2013) and Kepler et al. (2013), when examining each white dwarf candidate spectrum by eye, we found 206 stars with Zeeman splittings indicating magnetic fields above 2 MG – the limit below which we cannot identify since the line splitting is too small for the SDSS spectral resolution. If not identified as magnetic in origin, the spectra fittings of DA and DB models would have rendered too high $\log g$ determinations due to magnetic broadening being misinterpreted as pressure broadening. We also identified one DZH, in the same line as the DAZH identified by Kawka & Vennes (2014). We estimated the mean fields following Külebi et al. (2009), from 2 to 310 MG. We caution that stars with large fields are difficult to identify because any field above around 30 MG, depending on effective temperature and signal to noise, destroys the normal line sequences and affect the colours significantly. Additionally, the fields above 100 MG represent the so-called intermediate regime in which the magnetic white dwarf spectra have very few features, save the

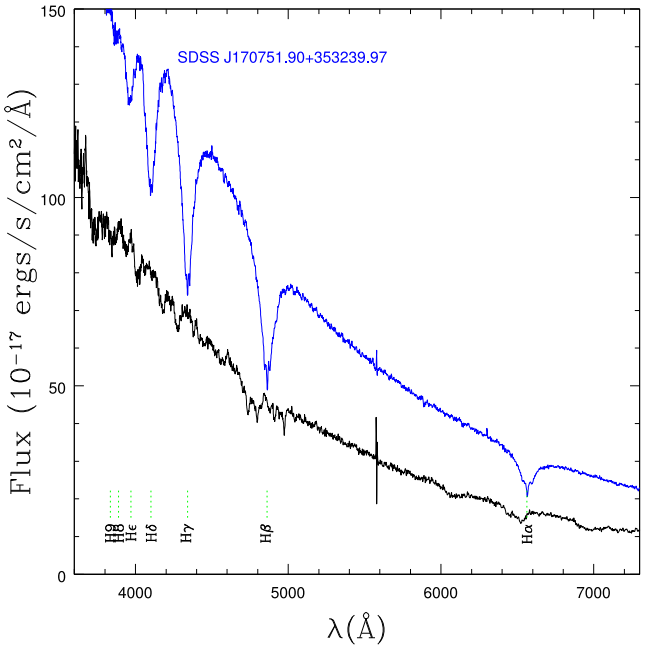

Figure 2. Spectra of the DAH SDSS J155708.04+041156.52, with a mean magnetic field $B = 41$ MG (bottom) and SDSS J170751.90+353239.97, with $B = 2.7$ MG (top).

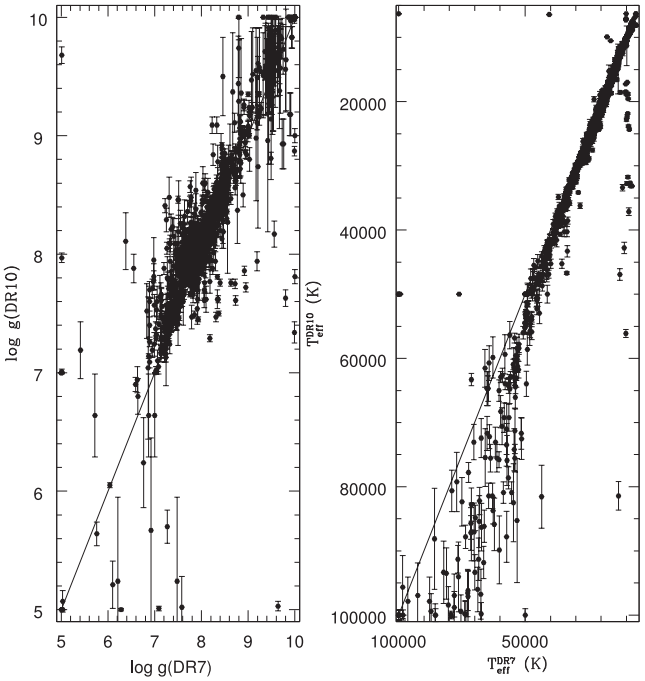

Figure 3. Surface gravities and effective temperature determinations for the same DA white dwarfs but with spectra obtained with the SDSS spectrograph (DR7) and the BOSS spectrograph (DR10), with slightly larger resolution and wavelength coverage.

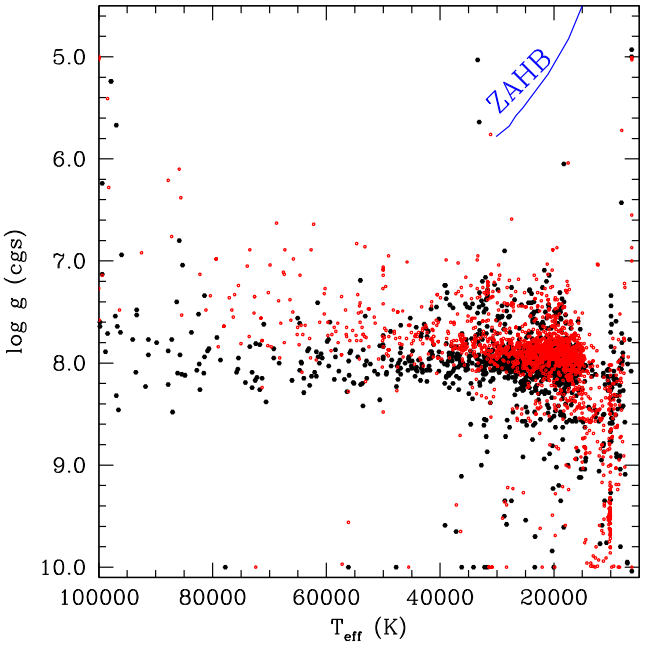

Figure 4. Surface gravities and effective temperature determinations for the same DA white dwarfs but with spectra obtained with the SDSS spectrograph (open circles, DR7) and the BOSS spectrograph (filled circles, DR10), with slightly larger resolution and wavelength coverage. There is a systematic shift to higher gravities in the DR10 observations. The line at the top right, marked ZAHB, shows the maximum $\log g$ a subdwarf can reach.

stationary transitions which have similar wavelengths for a distribution of magnetic fields.

Fig. 2 shows the S/N$_g$=42 and 58 spectra of the DAHs SDSS J155708.04+041156.52, with a mean magnetic field $B = 41$ MG, and SDSS J170751.90+353239.97, also known as GD 359, with a mean field of 2.7 MG. For the magnetic fields 2–100 MG most relevant for magnetic white dwarfs, the quadratic Zeeman effect is applicable. For this regime, not only the spectral line is divided into several components, the central component is also displaced with respect to its non-magnetic value.

4.3 Masses

Kleinman et al. (2013) limited the white dwarf classification in the lower limit of surface gravity to $\log g = 6.5$. At the cool end of our sample, $\log g = 6.5$ corresponds to a mass around 0.2 M$_\odot$, well below the single mass evolution in the lifetime of the Universe, which corresponds to $\simeq 0.45$ M$_\odot$, depending on the progenitor metallicity. All stars that form white dwarfs with masses below $\simeq 0.45$ M$_\odot$ should be the byproduct of binary star evolution involving interaction between the components, otherwise its lifetime on the main sequence would be larger than the age of the Universe.

DA white dwarf stars with $\log g \leq 6.5$ and $T_{\rm eff} < 20\,000$ K are DA-ELM (extreme low mass) as found by Brown et al. (2010, 2012, 2013) and Kilic et al. (2011, 2012). Hermes et al. (2012, 2013a,b) found pulsations in five of these ELMs, similar to those of DAVs (Van Grootel et al. 2013).

As a comparison of the DR7 and DR10 results, we plot in Figs 3 and 4 the $\log g$ and $T_{\rm eff}$ determinations of 1759 DAs observed in Ancillary Program 43, i.e. for which new spectra with BOSS was obtained of stars already observed with the SDSS spectrograph. Only 88 spectra have differences larger than 20 per cent, mainly at the high-temperature end and around 17 000 K $\geq T_{\rm eff} \geq$ 10 000 K, where there are two solutions in the spectral fittings, but there is a systematic shift of the DR10 observations to higher surface gravity, possibly caused by systematics in the flux calibrations (Genest-Beaulieu & Bergeron 2014).

Fig. 5 shows the surface gravity ($\log g$, in cgs units) as a function of the effective temperature ($T_{\rm eff}$, in K), estimated for all DAs

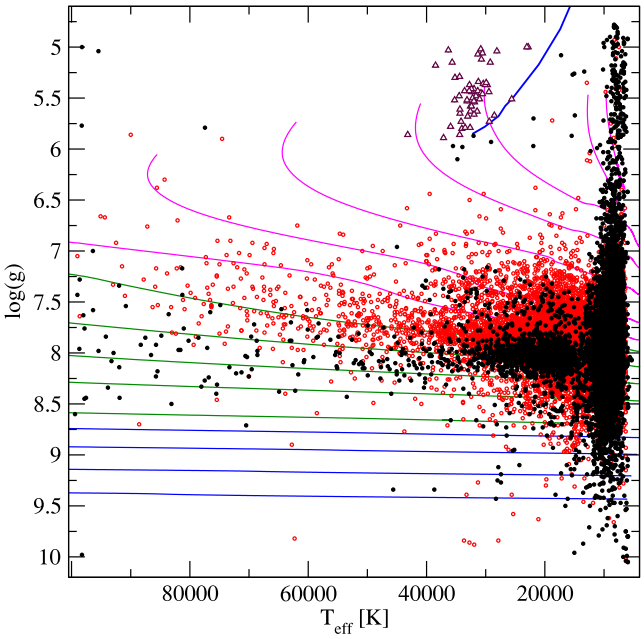

Figure 5. Surface gravity ($\log g$) and effective temperature ($T_{\rm eff}$) estimated for the new DA white dwarf stars with spectra with S/N$_g \geq 10$, with atmospheric models corrected to three-dimensional convection using the corrections reported in Tremblay et al. (2013, black dots). The decrease in the number of DAs between 15 000 K $\geq T_{\rm eff} \geq$ 11 000 K is caused by selection effects – the targeting for new white dwarfs selected only DAs hotter than 14 000 K. In open circles (red), we show the values for the DR7 DAs, but also corrected to three-dimensional convection using the corrections reported in Tremblay et al. (2013). It is evident that the surface gravities determined for the stars observed with the BOSS spectrograph, covering a larger wavelength range, resulted in slightly higher surface gravities. The zero-age horizontal branch (ZAHB) plotted was calculated specifically for this paper, with solar composition models. It indicates the highest possible surface gravity for a subdwarf. Stars with $T_{\rm eff} \leq 45\,000$ K and lower surface gravity than the ZAHB are sdBs, indicated with triangles in the figure. The low masses at the cool end are ELM white dwarfs, byproduct of binary evolution. The model lines show the ELM are concentrated at low effective temperatures. They are present even when we restrict our spectra to the 852 DAs with S/N $\geq$ 25, or even to the 125 with S/N $\geq$ 50.

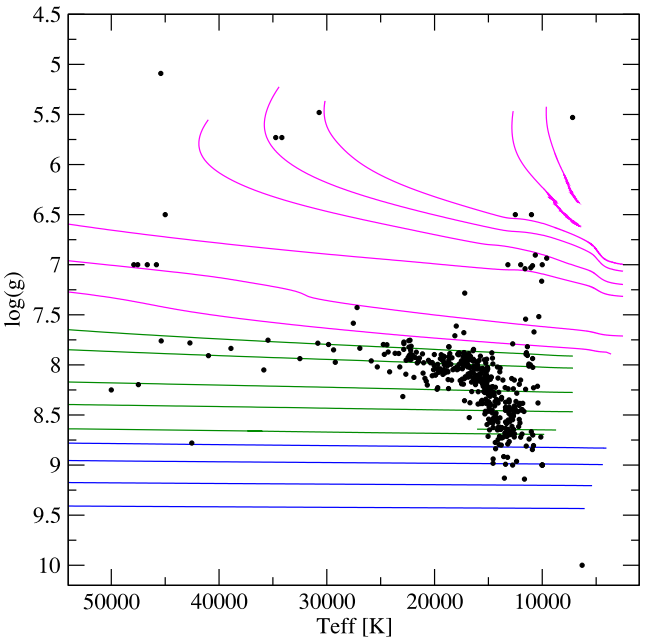

Figure 6. Surface gravity ($\log g$) and effective temperature ($T_{\rm eff}$) estimated for the new DB white dwarf stars from models with convection described by ML2/α=1.25 (black dots). Also plotted are full white dwarf evolutionary tracks. Carbon/oxygen sequences (green lines) correspond to He-rich atmosphere models with stellar mass ranging from 0.515 (top) to 0.87 M$_\odot$, while helium- (magenta) and oxygen/neon-core (blue, bottom) sequences correspond to DA white dwarf models (see the text for details). We see a rise in $\log g$ for DBs cooler than $T_{\rm eff} = 16\,000$ K, similar to that reported by Kepler et al. (2007) and also seen in fig. 21 of Bergeron et al. (2011), probably caused by incorrect neutral broadening modelling.

corrected to three-dimensional convection models using the corrections presented in Tremblay et al. (2013), and Fig. 6 for DBs with ML2/$\alpha = 1.25$.

We use the mass–radius relations of Renedo et al. (2010) and Romero, Campos & Kepler (2014) carbon–oxygen DA white dwarfs, for solar metallicities, to calculate the mass of our identified clean DA stars from the $T_{\rm eff}$ and $\log g$ values obtained from our fits, corrected to 3D convection. These relations are based on full evolutionary calculations appropriate for the study of hydrogen-rich DA white dwarfs that take into account the full evolution of progenitor stars, from the zero-age main sequence, through the hydrogen and helium central burning stages, thermally pulsating and mass-loss in the asymptotic giant branch phase and finally the planetary nebula domain. The stellar mass values for the resulting sequences range from 0.525 to 1.024 M$_\odot$, covering the stellar mass range for carbon–oxygen core DAs. For high-gravity white dwarf stars, we employed the mass–radius relations for O–Ne core white dwarfs given in Althaus et al. (2005) in the mass range from 1.06 to 1.30 M$_\odot$ with a step of 0.02 M$_\odot$. For the low-gravity white dwarf stars, we used the evolutionary calculations of Althaus, Miller Bertolami & Córsico (2013) for helium-core white dwarfs with stellar mass between 0.155 and 0.435 M$_\odot$, supplemented by sequences of 0.452 and 0.521 M$_\odot$ calculated in Althaus et al. (2009a).

For DB white dwarfs stars, we relied on the evolutionary calculations of hydrogen-deficient white dwarf stars with stellar mass between 0.515 and 0.870 M$_\odot$ computed by Althaus et al. (2009b). These sequences have been derived from the born-again episode responsible for the hydrogen deficient white dwarfs. For high- and low-gravity DBs, we used the O–Ne and helium evolutionary sequences, described before.

To calculate reliable mass distributions, we selected only the best S/N spectra with temperatures well fitted by our models. We find that reliable classifications that can be had from spectra with S/N $\geq$ 10. We classified 6243 spectra as clean DAs. Of these DAs, 2074 have a spectrum with S/N $\geq$10, with a mean S/N=25 $\pm$ 13 and $\langle \log g_{\rm DA} \rangle = 7.937 \pm 0.012$. Table 2 presents the mean masses for different signal-to-noise limits, after correcting to 3D convection models.

Table 2. Mean masses for DAs, corrected to 3D convection.

S/N$_g$	N	$\langle M_{\rm DA} \rangle$ (M$_\odot$)	N	$\langle M_{\rm DA} \rangle$ $T_{\rm eff} \geq 10\,000$ K (M$_\odot$)
10	2074	0.626 $\pm$ 0.004	1573	0.659 $\pm$ 0.003
15	1659	0.656 $\pm$ 0.004	1484	0.662 $\pm$ 0.003
25	852	0.669 $\pm$ 0.005	821	0.677 $\pm$ 0.005
50	125	0.663 $\pm$ 0.014	120	0.679 $\pm$ 0.011

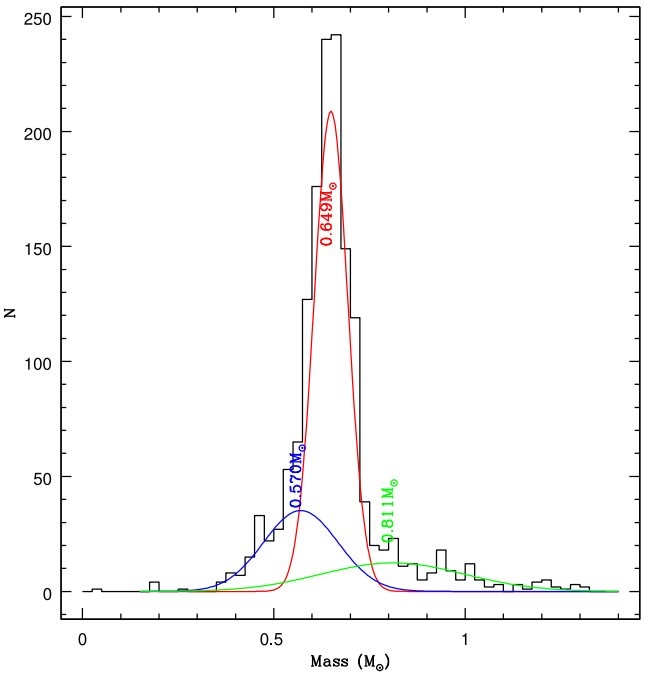

Figure 7. Histogram for the mass distribution of S/N $\geq$ 10 and $T_{\rm eff} \geq 12\,000$ K DAs versus mass, for log g corrected to three-dimensional convection models using the corrections reported in Tremblay et al. (2013). Even though the mass histogram is not expected to have a Gaussian shape, we have decomposed it in three Gaussians, just as a guide: $N = 208.9^{*}\exp[-(M-0.649)^2/(2^{*}0.044^2)] + 35.2^{*}\exp[-(M-0.570)^2/(2^{*}0.097^2)] + 12.4^{*}\exp[-(M-0.811)^2/(2^{*}0.187^2)]$. As in Kepler et al. (2007) and Kleinman et al. (2013), we find a significant number of stars with masses below 0.45 $M_{\odot}$, product of interacting binary evolution.

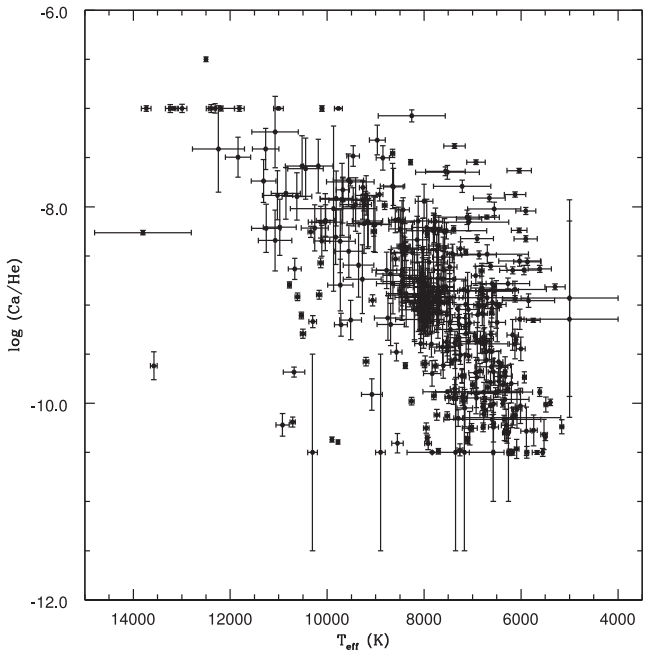

Figure 8. Calcium/helium abundances estimated for DZs, assuming a bulk Earth composition for the accreted material.

The mean masses estimated in this sample are larger than those obtained by Kleinman et al. (2013), which did not use the 3D correction, but now closer to the results of other determinations methods, as gravitational redshift (Falcon et al. 2010) and seismology (Romero et al. 2012), and especially with the Gianninas, Bergeron & Ruiz (2011) sample of bright DAs corrected to 3D by Tremblay et al. (2013) which is centred at 0.637 $M_{\odot}$.

Fig. 7 shows the mass histogram for the 1 504 DAs with S/N $\geq$ 10 and $T_{\rm eff} \geq 12\,000$ K.

The spectra we classified as clean DBs belong to 381 stars. 373 of these have a spectral S/N $\geq$10, with a mean S/N=25 $\pm$ 11. Using this high S/N sample, we obtain $\langle \log g_{\rm DB} \rangle = 8.122 \pm 0.017$. and a corresponding mean mass of $\langle M_{\rm DB} \rangle = 0.696 \pm 0.010\,M_{\odot}$, similar to the results from gravitational redshift by Falcon et al. (2012) and Bergeron et al. (2011), and to $\langle M_{\rm DB} \rangle = 0.685 \pm 0.013\,M_{\odot}$ for the 191 DBs with S/N$\geq$15 of Kleinman et al. (2013).

4.4 DZs

9 per cent of white dwarfs cooler than $T_{\rm eff} = 12\,000$ K in our sample show spectra contaminated by metals, probably due to accretion of rocky material around the stars (e.g. Graham et al. 1990; Jura 2003; Koester, Gänsicke & Farihi 2014). Calcium and magnesium in general have the strongest lines for white dwarfs at these temperatures.

We fitted the spectra of each of the 397 stars classified as DZs to a grid of models with Mg, Ca and Fe ratios equal to the averages from the cool DZ in Koester et al. (2011), and Si added with the same abundance as Mg. This is fairly close to bulk Earth, except for the missing oxygen (Koester et al. 2014). The models have fixed surface gravity at log $g = 8.0$ as it is not possible to estimate it from the spectra. The absolute values for log Ca/He range from -7.25 to -10.50. Fig. 8 shows the calcium/helium abundance for the 397 DZs identified. There seems to be a decrease of Ca/He abundances at lower temperatures, that could be explained by approximately the same accretion rate diluted by increasing convection layer.

4.5 DQs

1 per cent of white dwarfs cooler than $T_{\rm eff} = 12\,000$ K in our sample show spectra dominated by carbon lines, probably due to dredge-up of carbon from the underlying carbon–oxygen core through the expanding He convection zone (e.g. Koester, Weidemann & Zeidler 1982; Pelletier et al. 1986; Koester & Knist 2006; Dufour et al. 2007).

We fitted the spectra of the stars classified as cool DQs to a grid of models reported by Koester & Knist (2006). The models have fixed surface gravity at log $g = 8.0$ as it is not possible to estimate it from the spectra. The absolute values for log C/He range from -8 to -4, and effective temperatures from 13 000 to 4400 K. The hotter DQs were fitted with the models of Dufour (2011) and Dufour et al. (2013). Fig. 9 shows the carbon/helium abundance for the 71 DQs identified.

4.6 White dwarf-main-sequence binaries

We have identified 180 white dwarfs that are part of binary systems containing main-sequence companions (WDMS binaries), of which 171 are not included in the latest version of the SDSS WDMS binary catalogue (Rebassa-Mansergas et al. 2013). Li et al. (2014) report 227 DR9 DA+M pairs, 111 of which also found by us independently. The majority of our new systems contain a DA white dwarf and an M dwarf secondary star (DA+M, see Table 3), and we measure their stellar parameters following the decomposition/fitting

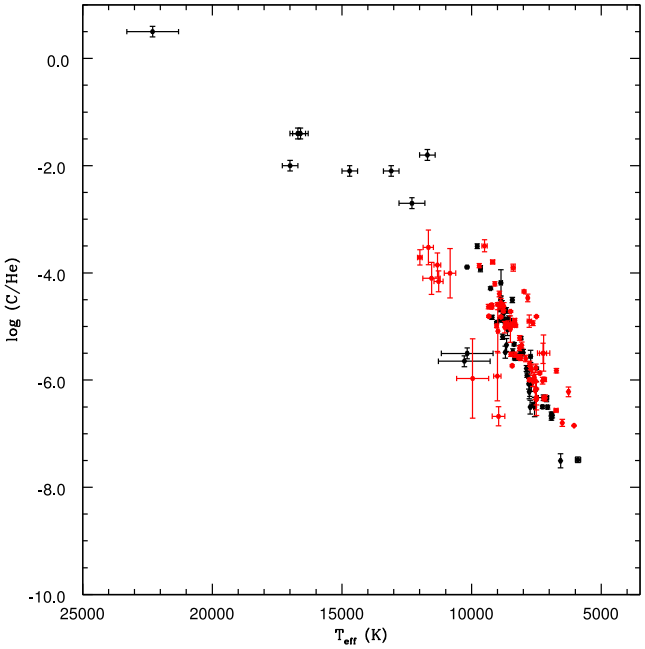

Figure 9. Carbon/helium abundances estimated for DQs. The increase with decreasing temperature comes from the increase in transparency and deepening convection zone. The lighter (red) points are the results of our fits with the same models for the cool DQs in Kleinman et al. (2013).

Table 3. Number of newly identified WDMS binary by types.

Classification	Number	Classification	Number
DA+M	127	DB+M?	1
DA+M:	12	DB:/M	2
DA/K	2	DB:?	1
DA:+M	2	DBA+M	1
DB+?	1	DC+M	2
DB+K	1	DC+M:	2
DB+M	12	DA/F	1

routine described in Rebassa-Mansergas et al. (2007). In a first step, a given WDMS binary spectrum is fitted with a combination of M dwarf plus white dwarf templates and the spectral type of the M dwarf is determined. The best-fitting M dwarf template is then subtracted and the residual white dwarf spectrum is fitted with the model grid of DA white dwarfs of Koester (2010). The fits to the normalized Balmer lines are used to derive the white dwarf effective temperature and surface gravity, and the fit to the entire spectrum (continuum plus lines) is used to break the degeneracy between the hot and cold solutions. The 3D corrections of Tremblay et al. (2013) are applied to our white dwarf parameter determinations. The stellar parameters are provided in Table 6.

76 of the new DA+M binaries in our sample have spectra with SN $\geq$10, and for 74 (73) of them, we derive reliable white dwarf parameters (M dwarf spectral types) fitting their SDSS spectra (Table 6). The parameter distributions are shown in Fig. 10, left-hand panels. On the right-hand panels of the same figure, we show the cumulative parameter distributions, which are compared to those obtained from the latest version of the SDSS (DR8) WDMS binary catalogue (Rebassa-Mansergas et al. 2013). For a meaningful comparison, we apply the 3D corrections of Tremblay et al. (2013) to

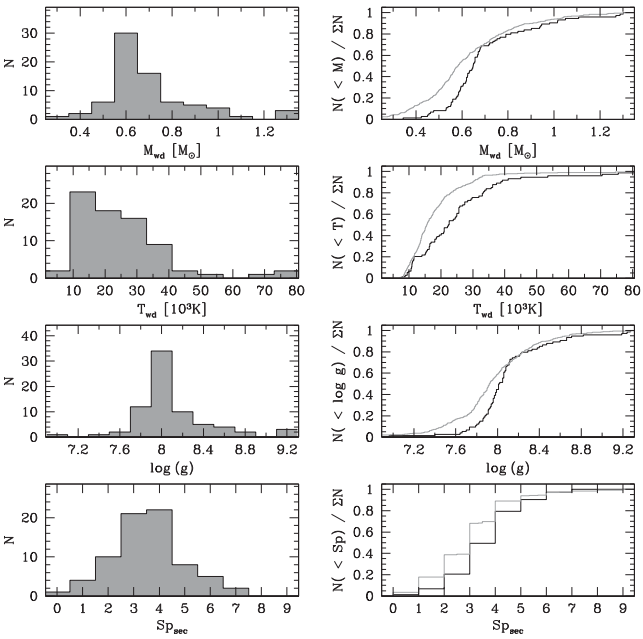

Figure 10. Left-hand panels: distribution of white dwarf mass (top), effective temperature (middle-top) and surface gravity (middle-bottom) and M dwarf spectral type (bottom) of new WDMS binaries identified in this work with spectra of SN $\geq$10. Right-hand panels: the cumulative parameter distributions, in the same order as in the left-hand columns (black lines). The cumulative parameter distributions of the DR8 WDMS binary catalogue are shown in grey (only parameters obtained from spectra of SN $\geq$10 are considered).

the DR8 data as well as consider only systems with spectra of SN $\geq$10. Inspection of the cumulative distributions of both studies reveals that white dwarfs presented here in the WDMS binary sample are systematically hotter (middle-top right-hand panel of Fig. 10), and that there is a clear lack of low-mass white dwarfs in the DR10 sample as compared to the DR8 catalogue (top and middle-bottom right-hand panels of Fig. 10). The fraction of early-type M dwarfs is lower in the DR10 WDMS binary sample (Fig. 10, bottom panel).

4.7 Subdwarfs

Hot subdwarfs are core He burning stars. Following Németh, Kawka & Vennes (2012), Drilling et al. (2013) and Nemeth et al. (2014a,b), we have classified stars with $\log g < 6.5$ as hot subdwarfs; sdOs if He II present and sdBs if not, between 45 000 K $> T_{\rm eff} >$ 20 000 K. Nemeth et al. (2014a) and Rauch et al. (2014) discuss how the He abundances typical for sdB stars affect the NLTE atmosphere structure, and to a lower extent CNO and Fe abundances are also important in deriving accurate temperatures and gravities. Our determinations of $T_{\rm eff}$ and $\log g$ do not include NLTE effects or mixed compositions, so they serve only as a rough indicator. Stars with $6.5 > \log g > 5.0$ and $T_{\rm eff} <$ 20 000 K were labelled ELM-DAs, as they lay below the ZAHB (Dreizler et al. 2002; Althaus et al. 2013; Gianninas et al. 2014). Of the 647 sds, we classified 262 sdOs and 375 sdBs. We also identified $\simeq$ 200 stars with $\log g < 5.2$ as either main-sequence stars (Arnold & Gilmore 1992), even though their implied distance moduli would be larger than $m - M = 16.5$ and most of them have Galactic latitude $b > 10$ deg, or more likely as ELM white dwarfs (Brown et al. 2010, 2012, 2013; Kilic et al. 2012).

Table 4. Featureless spectra objects that have radio emission consistent with BL Lac classification. Four objects associated with some amount of proper motion, SDSS J091141.72+424844.17, SDSSJ150716.42+172102.89, SDSS J163506.77+345852.24 and SDSS J220812.70+035304.61, are most likely BL Lacs given their clearly non-thermal broad-band spectral energy distribution. In all these cases, the measured proper motion is not highly statistically significant and could have been affected by strong variability that is typical of BL Lacs. All these eight objects have H(21 cm) column densities larger than 10^{20} cm^{-2} and most show variability in the Catalina Sky Survey (Drake et al. 2012).

P-M-F	SDSS J	S/N	*u*	*g*	*r*	*i*	*z*	ppm (mas yr^{-1})	aro	Radio flux (mJy, 1.4 GHz)
4394–55924–0742	021311.76−050102.56	21	20.42 ± 00.06	19.95 ± 00.02	19.54 ± 00.02	19.20 ± 00.02	18.87 ± 00.04	0	0.500	32
4342–55531–0304	024519.63−025628.12	29	19.48 ± 00.03	18.96 ± 00.01	18.55 ± 00.01	18.24 ± 00.01	17.95 ± 00.02	0	0.491	74
3802–55528–0818	080551.76+383538.04	17	21.64 ± 00.11	20.99 ± 00.04	20.38 ± 00.03	19.94 ± 00.03	19.59 ± 00.07	0	0.488	13
4603–55999–0880	091141.72+424844.17	16	20.60 ± 00.05	20.11 ± 00.02	19.72 ± 00.02	19.37 ± 00.02	19.10 ± 00.04	7 ± 3	0.516	34
5399–55956–0224	122307.25+110038.28	23	19.89 ± 00.04	19.61 ± 00.01	19.39 ± 00.01	19.13 ± 00.02	19.00 ± 00.04	0	0.250	2
5484–56039–0716	150716.42+172102.89	15	19.74 ± 00.03	19.40 ± 00.01	19.03 ± 00.01	18.77 ± 00.01	18.64 ± 00.03	12 ± 6	0.439	23
5188–55803–0712	163506.77+345852.24	14	20.76 ± 00.06	20.29 ± 00.02	19.83 ± 00.02	19.49 ± 00.02	19.15 ± 00.05	11 ± 4	0.578	66
4318–55508–0464	220812.70+035304.61	17	19.85 ± 00.04	19.40 ± 00.01	18.92 ± 00.01	18.59 ± 00.01	18.29 ± 00.03	20 ± 17	0.465	40

Table 5. Columns provided in data table, Table 6.

Column no.	Heading	Description
1	Name	SDSS object name (SDSS 2000J+)
2	P-M-F	SDSS Plate number–Modified Julian Date–Fibre
3	SN_g	SDSS *g*-band signal-to-noise ratio
4	u_psf	SDSS *u*-band PSF magnitude
5	u_err	SDSS *u*-band uncertainty
6	g_psf	SDSS *g*-band PSF magnitude
7	g_err	SDSS *g*-band uncertainty
8	r_psf	SDSS *r*-band PSF magnitude
9	r_err	SDSS *r*-band uncertainty
10	i_psf	SDSS *i*-band PSF magnitude
11	i_err	SDSS *i*-band uncertainty
12	z_psf	SDSS *z*-band PSF magnitude
13	z_err	SDSS *z*-band uncertainty
14	PM	SDSS proper motion (0.01 yr^{-1})
15	T_eff	$T_{\rm eff}$
16	T_err	$T_{\rm eff}$ uncertainty
17	log_g	log *g*
18	log_gerr	log *g* uncertainty
19	humanID	Human classification
20	T_eff (3D)	$T_{\rm eff}$ for pure DAs and DBs or −log(Ca/He) for DZs or −log(C/He) for DQs[a]
21	T_err (3D)	$T_{\rm eff}$ uncertainty
22	log_g (3D)	log *g*
23	log_gerr (3D)	log *g* uncertainty
24	Mass	Calculated mass ($M_\odot$)
25	Mass_err	Mass uncertainty ($M_\odot$)

[a]The temperatures and surface gravities are corrected to the three-dimensional convection models of Tremblay et al. (2013). The Ca/He and C/He abundances, calculated assuming log *g* = 8.0, are indicated by −log(Ca/He) or −log(C/He).

4.8 DCs and BL Lac

Featureless optical spectra are typical of DC white dwarfs, but also from extragalactic BL Lac objects. BL Lac objects are strong sources of radio, while non-interacting DCs are not. DCs, if bright enough to be detected in all images, should have measurable proper motions, as they are cool faint objects. To separate these objects, we searched for 1.4 GHz radio emission in the literature. BL Lac objects have in general a power-law spectra from optical to radio, with a radio to optical exponent larger than aro = 0.250. We found 67/260 objects we had classified by eye the spectrum as DCs are in fact known BL Lac objects. We also found eight objects, listed in Table 4, with measured radio flux compatible with them being BL Lac objects.

Table 5 lists the columns of data provided in our electronic catalogue file, Table 6.

5 CONCLUSIONS AND DISCUSSION

We have identified 9088 new white dwarf and subdwarf stars in the DR10 of the SDSS, and estimated the mean masses for DAs and DBs, as well as the calcium contamination in DZs and carbon in DQs. We were able to extend our identifications down to $T_{\rm eff}$ = 5000 K, although certainly not complete, as we relied also on proper motion measurements, which are incomplete below *g*

Table 6. New white dwarf stars. Notes: P-M-F are the Plate–Modified Julian Date–Fibre number that designates an SDSS spectrum. A: designates an uncertain classification. The columns are fully explained in Table 5. When $\sigma(\log g) = 0.000$, we have assumed $\log g = 8.0$, not fitted the surface gravity. The full table is available online.

#SDSS J	Plate-MJD-Fiber	S/N	u	su	g	sg	r	sr	i	si	z	si	ppm	Teff	sTeff	logg	slogg	Type	T(3D)	sT	logg	slogg	Mass	sMass
#			(mag)	(mag)	(mag)	(mag)	(mag)	(mag)	(mag)	(mag)	(mag)	(mag)	0.01" /yr	(K)	(K)	(cgs)	(cgs)		(K)	(K)	(cgs)	(cgs)	(Msun)	(Msun)
#																								
000111.66+000342.55	4216-55477-0816	019	19.21	00.03	19.26	00.03	19.33	00.02	19.39	00.03	19.55	00.06	00.00	11323	00124	8.000	0.000	DB						
000116.49+000204.45	4216-55477-0200	026	18.87	00.02	18.78	00.01	18.90	00.01	19.04	00.01	19.23	00.05	05.46	11107	00090	8.000	0.000	DBA						
000216.03+120309.36	5649-55912-0467	002	22.88	00.43	22.02	00.08	21.97	00.11	22.20	00.19	22.38	00.61	00.00	10464	00433	8.584	0.212	DA	10422	00433	8.310	0.210	0.787	0.130
000243.16+073856.25	4535-55860-0842	045	17.67	00.01	17.52	00.01	17.86	00.01	18.11	00.01	18.38	00.02	01.41	20153	00080	8.178	0.001	DA	20153	00080	8.180	0.000	0.716	0.000
000247.21+101144.16	4534-55863-0584	013	20.84	00.07	19.71	00.02	19.00	00.02	18.88	00.02	18.76	00.04	00.00	06302	00006	5.430	0.240	DAZ:						
000257.88+114719.07	5649-55912-0400	001	23.05	00.53	22.21	00.09	21.94	00.12	22.32	00.22	22.57	00.65	00.00	12628	01528	9.380	0.400	DA	12862	01528	9.190	0.400	1.237	0.136
000307.89+111732.42	5649-55912-0384	002	22.71	00.37	21.95	00.08	21.79	00.11	21.93	00.16	21.04	00.27	00.00	10235	00353	8.377	0.352	DA	10190	00353	8.100	0.350	0.657	0.190
000310.38+071801.11	4535-55860-0159	030	18.11	00.01	18.28	00.01	18.68	00.01	18.96	00.01	19.24	00.06	01.89	30455	00130	8.116	0.003	DA	30455	00130	8.120	0.000	0.705	0.000
000316.36+133829.22	5649-55912-0584	001	23.03	00.98	22.20	00.07	22.21	00.13	22.62	00.30	21.96	00.52	00.00	11045	00636	7.932	0.429	DA	11136	00636	7.740	0.430	0.490	0.180
000321.60-015310.86	4365-55539-0502	015	19.24	00.03	19.19	00.01	19.30	00.01	19.48	00.02	19.71	00.07	05.00	06039	01000	7.984	0.431	DA-He	06050	01000	7.990	0.430	0.584	0.225

$\simeq 21$. The substantial increase in the number of spectroscopically confirmed white dwarfs is important because it allows the discovery of the rare objects, like the massive white dwarfs and oxygen spectrum over helium-dominated atmosphere ones. The improvements in the signal to noise and spectral coverage of BOSS spectra versus the SDSS spectrograph also allowed for improvements in the stellar parameters, though systematic effects mainly due to flux calibration must be explored.

ACKNOWLEDGEMENTS

SOK, IP, GO, ADR and JESC are supported by CNPq and FAPERGS-Pronex-Brazil. DK received support from programme Science without Borders, MCIT/MEC-Brazil. BK is supported by the MICINN grant AYA08-1839/ESP, by the ESF EUROCORES Program EuroGENESIS (MICINN grant EUI2009-04170), by the 2009SGR315 of the Generalitat de Catalunya and EU-FEDER funds. ARM acknowledges financial support from the Postdoctoral Science Foundation of China (grants 2013M530470 and 2014T70010) and from the Research Fund for International Young Scientists by the National Natural Science Foundation of China (grant 11350110496).

Funding for SDSS-III has been provided by the Alfred P. Sloan Foundation, the Participating Institutions, the National Science Foundation and the US Department of Energy Office of Science. The SDSS-III website is http://www.sdss3.org/.

SDSS-III is managed by the Astrophysical Research Consortium for the Participating Institutions of the SDSS-III Collaboration including the University of Arizona, the Brazilian Participation Group, Brookhaven National Laboratory, Carnegie Mellon University, University of Florida, the French Participation Group, the German Participation Group, Harvard University, the Instituto de Astrofisica de Canarias, the Michigan State/Notre Dame/JINA Participation Group, Johns Hopkins University, Lawrence Berkeley National Laboratory, Max Planck Institute for Astrophysics, Max Planck Institute for Extraterrestrial Physics, New Mexico State University, New York University, Ohio State University, Pennsylvania State University, University of Portsmouth, Princeton University, the Spanish Participation Group, University of Tokyo, University of Utah, Vanderbilt University, University of Virginia, University of Washington and Yale University.

REFERENCES

Abazajian K. et al., 2003, AJ, 126, 2081
Abazajian K. N. et al., 2009, ApJS, 182, 543
Adelman-McCarthy J. K. et al., 2006, ApJS, 162, 38
Ahn C. P. et al., 2014, ApJS, 211, 17
Althaus L. G., García-Berro E., Isern J., Córsico A. H., 2005, A&A, 441, 689
Althaus L. G., Panei J. A., Romero A. D., Rohrmann R. D., Córsico A. H., García-Berro E., Miller Bertolami M. M., 2009a, A&A, 502, 207
Althaus L. G., Panei J. A., Miller Bertolami M. M., García-Berro E., Córsico A. H., Romero A. D., Kepler S. O., Rohrmann R. D., 2009b, ApJ, 704, 1605
Althaus L. G., Miller Bertolami M. M., Córsico A. H., 2013, A&A, 557, A19
Arnold R., Gilmore G., 1992, MNRAS, 257, 225
Bergeron P. et al., 2011, ApJ, 737, 28
Bolton A. S. et al., 2012, AJ, 144, 144
Brown W. R., Kilic M., Allende Prieto C., Kenyon S. J., 2010, ApJ, 723, 1072

Brown W. R., Kilic M., Allende Prieto C., Kenyon S. J., 2012, ApJ, 744, 142
Brown W. R., Kilic M., Allende Prieto C., Gianninas A., Kenyon S. J., 2013, ApJ, 769, 66
Dawson K. S. et al., 2013, AJ, 145, 10
Denissenkov P. A., Herwig F., Truran J. W., Paxton B., 2013, ApJ, 772, 37
Denissenkov P., Truran J. W., Herwig F., Jones S., Paxton B., Nomoto K., Suzuki T., Toki H., 2014, preprint (arXiv:1407.0248)
Doherty C. L., Gil-Pons P., Siess L., Lattanzio J. C., Lau H. H. B., 2014, preprint (arXiv:1410.5431)
Drake A. J. et al., 2012, in Griffin E., Hanisch R., Seaman R., eds, Proc. IAU Symp. 285, New Horizons in Time-Domain Astronomy. Cambridge Univ. Press, Cambridge, p. 306
Dreizler S., Schuh S. L., Deetjen J. L., Edelmann H., Heber U., 2002, A&A, 386, 249
Drilling J. S., Jeffery C. S., Heber U., Moehler S., Napiwotzki R., 2013, A&A, 551, A31
Dufour P., 2011, in Hoard D. W., ed., White Dwarf Atmospheres and Circumstellar Environments. Wiley, New York, p. 53
Dufour P., Liebert J., Fontaine G., Behara N., 2007, Nature, 450, 522
Dufour P., Vornanen T., Bergeron P., Fontaine B. A., 2013, in Krzesiński J., Stachowski G., Moskalik P., Bajan K., eds, ASP Conf. Ser. Vol. 469, 18th European White Dwarf Workshop. Astron. Soc. Pac., San Francisco, p.167
Eisenstein D. J. et al., 2006, ApJS, 167, 40
Eisenstein D. J. et al., 2011, AJ, 142, 72
Falcon R. E., Winget D. E., Montgomery M. H., Williams K. A., 2010, ApJ, 712, 585
Falcon R. E., Winget D. E., Montgomery M. H., Williams K. A., 2012, ApJ, 757, 116
Gänsicke B. T., Koester D., Girven J., Marsh T. R., Steeghs D., 2010, Science, 327, 188
Genest-Beaulieu C., Bergeron P., 2014, ApJ, 796, 128
Gianninas A., Bergeron P., Ruiz M. T., 2011, ApJ, 743, 138
Gianninas A., Dufour P., Kilic M., Brown W. R., Bergeron P., Hermes J. J., 2014, ApJ, 794, 35
Graham J. R., Matthews K., Neugebauer G., Soifer B. T., 1990, ApJ, 357, 216
Harris H. C. et al., 2003, AJ, 126, 1023
Hermes J. J., Montgomery M. H., Winget D. E., Brown W. R., Kilic M., Kenyon S. J., 2012, ApJ, 750, L28
Hermes J. J. et al., 2013a, ApJ, 765, 102
Hermes J. J. et al., 2013b, MNRAS, 436, 3573
Jura M., 2003, ApJ, 584, L91
Kawka A., Vennes S., 2014, MNRAS, 439, L90
Kepler S. O., Kleinman S. J., Nitta A., Koester D., Castanheira B. G., Giovannini O., Costa A. F. M., Althaus L., 2007, MNRAS, 375, 1315
Kepler S. O. et al., 2013, MNRAS, 429, 2934
Kilic M., Brown W. R., Allende Prieto C., Agüeros M. A., Heinke C., Kenyon S. J., 2011, ApJ, 727, 3
Kilic M., Brown W. R., Allende Prieto C., Kenyon S. J., Heinke C. O., Agüeros M. A., Kleinman S. J., 2012, ApJ, 751, 141
Kleinman S. J. et al., 2004, ApJ, 607, 426
Kleinman S. J. et al., 2013, ApJS, 204, 5.
Koester D., 2010, Mem. Soc. Astron. Ital., 81, 921
Koester D., Knist S., 2006, A&A, 454, 951
Koester D., Weidemann V., Zeidler E.-M., 1982, A&A, 116, 147
Koester D., Girven J., Gänsicke B. T., Dufour P., 2011, A&A, 530, A114
Koester D., Gänsicke B. T., Farihi J., 2014, A&A, 566, A34
Külebi B., Jordan S., Euchner F., Gänsicke B. T., Hirsch H., 2009, A&A, 506, 1341
Li L., Zhang F., Han Q., Kong X., Gong X., 2014, MNRAS, 445, 1331
Monet D. G. et al., 2003, AJ, 125, 984
Napiwotzki R., 1997, A&A, 322, 256
Németh P., Kawka A., Vennes S., 2012, MNRAS, 427, 2180
Nemeth P., Östensen R., Vos J., Kawka A., Vennes S., 2014a, in van Grootel V., Green E., Fontaine G., Charpinet S., eds, ASP Conf. Ser. Vol. 481, 6th Meeting on Hot Subdwarf Stars and Related Objects. Astron. Soc. Pac., San Francisco, p. 75
Nemeth P., Östensen R., Tremblay P., Hubeny I., 2014b, in van Grootel V., Green E., Fontaine G., Charpinet S., eds, ASP Conf. Ser. Vol. 481, 6th Meeting on Hot Subdwarf Stars and Related Objects. Astron. Soc. Pac., San Francisco, p. 95
Nomoto K., 1984, ApJ, 277, 791
Pelletier C., Fontaine G., Wesemael F., Michaud G., Wegner G., 1986, ApJ, 307, 242
Rauch T., Rudkowski A., Kampka D., Werner K., Kruk J. W., Moehler S., 2014, A&A, 566, A3
Rebassa-Mansergas A., Gänsicke B. T., Rodríguez-Gil P., Schreiber M. R., Koester D., 2007, MNRAS, 382, 1377
Rebassa-Mansergas A., Agurto-Gangas C., Schreiber M. R., Gänsicke B. T., Koester D., 2013, MNRAS, 433, 3398
Reindl N., Rauch T., Werner K., Kepler S. O., Gänsicke B. T., Gentile Fusillo N. P., 2014, A&A, preprint (arXiv:1410.7666)
Renedo I., Althaus L. G., Miller Bertolami M. M., Romero A. D., Córsico A. H., Rohrmann R. D., García-Berro E., 2010, ApJ, 717, 183
Romero A. D., Córsico A. H., Althaus L. G., Kepler S. O., Castanheira B. G., Miller Bertolami M. M., 2012, MNRAS, 420, 1462
Romero A., Campos F., Kepler S. O., 2014, MNRAS, submitted
Si J., Luo A., Li Y., Zhang J., Wei P., Wu Y., Wu F., Zhao Y., 2014, Sci. China Phys., Mech. Astron., 57, 176
Smartt S. J., 2009, ARA&A, 47, 63
Smartt S. J., Eldridge J. J., Crockett R. M., Maund J. R., 2009, MNRAS, 395, 1409
Smee S. A. et al., 2013, AJ, 146, 32
Straniero O., Domínguez I., Imbriani G., Piersanti L., 2003, ApJ, 583, 878
Tremblay P.-E., Ludwig H.-G., Steffen M., Freytag B., 2013, A&A, 559, A104
Valenti S. et al., 2009, Nature, 459, 674
Van Grootel V., Fontaine G., Brassard P., Dupret M.-A., 2013, ApJ, 762, 57
Werner K., Rauch T., Kepler S. O., 2014, A&A, 564, A53

SUPPORTING INFORMATION

Additional Supporting Information may be found in the online version of this article:

Table 6. New white dwarf stars. Notes: P-M-F are the Plate–Modified Julian Date–Fibre number that designates an SDSS spectrum. A: designates an uncertain classification. The columns are fully explained in Table 5. When $\sigma(\log g) = 0.000$, we have assumed $\log g = 8.0$, not fitted the surface gravity. (http://mnras.oxfordjournals.org/lookup/suppl/doi:10.1093/mnras/stu2388/-/DC1).

Please note: Oxford University Press are not responsible for the content or functionality of any supporting materials supplied by the authors. Any queries (other than missing material) should be directed to the corresponding author for the article.

This paper has been typeset from a TEX/LATEX file prepared by the author.